Comparison of Analysis, Simulation, and Measurement of Wire-to-Wire Crosstalk, Part 1

Arthur T. Bradley[#1], Brian J. Yavoich[#2], Shane M. Hodson[#3], Richard F. Godley[#4]

NASA Langley Research Center

5 North Dryden, MS488, Hampton, VA 23681 USA

[1]arthur.t.bradley@nasa.gov

[2]brian.yavoich@fandm.edu

[3]smh7zy@virginia.edu

[4]rgodley@gmail.com

***Abstract*— In this investigation, we compare crosstalk analysis, simulation, and measurement results for electrically short configurations. Methods include hand calculations, PSPICE simulations, Microstripes transient field solver, and empirical measurement. In total, four representative physical configurations are examined, including a single wire over a ground plane, a twisted pair over a ground plane, generator plus receptor wires inside a cylindrical conduit, and a single receptor wire inside a cylindrical conduit. Part 1 addresses the first two cases, and Part 2 addresses the final two. Agreement between the analysis, simulation, and test data is shown to be very good.**

I. Introduction

Crosstalk is the unintended electromagnetic coupling between wires in close proximity. It is dependent on many factors including wire type, physical dimensions, spacing, surrounding materials, field type and levels, and frequencies. For electrically short wires, crosstalk can be modeled using simple lumped circuit analysis as well as more general transmission line techniques (1). It can also be simulated using transient field solver programs, such as Microstripes.

In this investigation, four different wire configurations were examined, including a single wire over a ground plane, a twisted pair over a ground plane, two wires (generator plus receptor) inside a cylindrical conduit, and a single wire inside a cylindrical conduit. The first two configurations are examined in this paper. The final two are examined in the Part 2 publication (also included in the proceedings of the 2010 Asia Pacific EMC Symposium). Hand calculations, simulations, and experimental results were compared and shown to agree very well.

As shown in Fig. 1, the crosstalk system consisted of a generator circuit (i.e. source wire) and a receptor circuit (i.e. victim wire). The generator circuit remained a simple single wire conductor over a ground plane for all experiments. The receptor wire configuration was varied for each test case. Both circuits were mounted over a flat heavy gauge aluminum reference conductor.

The generator stimulus was provided by the voltage source, V_S, injected at the near end and terminated into R_L. Electromagnetic fields, both E and H, coupled energy from the generator circuit into the receptor circuit. Some reverse coupling also occurred from receptor back to the generator circuit.

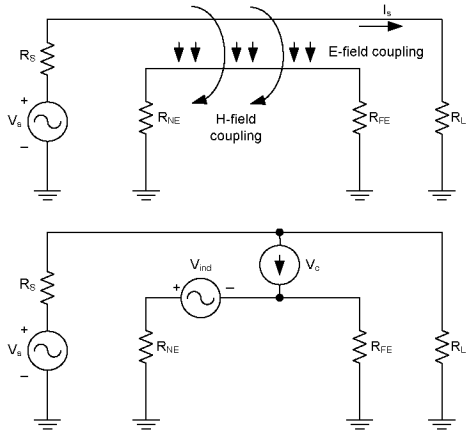

Fig. 1 Lumped circuit representation

The current driven by V_S in the generator circuit generates a time-varying electric field primarily perpendicular to the receptor wire, and a circulating magnetic field with flux lines that penetrate the loop formed by the receptor wire and reference conductor. Faraday's law is used to describe the relation of those fluxes to induced wire voltage. The E-field coupling is modeled by a wire-to-wire current source, and the H-field is modeled by a series voltage source.

Measurements of V_{NE} and V_{FE} were taken across R_{NE} and R_{FE} respectively. Resistors R_{NE} and R_{FE} were varied from 20Ω - 1960Ω, but always kept equal to each other. Resistor R_L was also independently varied. V_S was adjusted for every test case to apply a constant 1.75V amplitude 5MHz sinusoid across the load resistor, allowing the losses associated with R_S to be removed from the analysis.

The importance of this work is twofold. First, it clearly demonstrates the applicability (and limitations) of lumped circuit crosstalk analyses. It also identifies and discusses important crosstalk effects only discernible from varying system impedances. Such discussion is not typically included in prevalent literature which focuses instead on studying crosstalk across varying frequencies.

II. Single Wire Configuration

The single-wire experimental setup shown in Fig. 2 consisted of a simple electronic assembly with two parallel

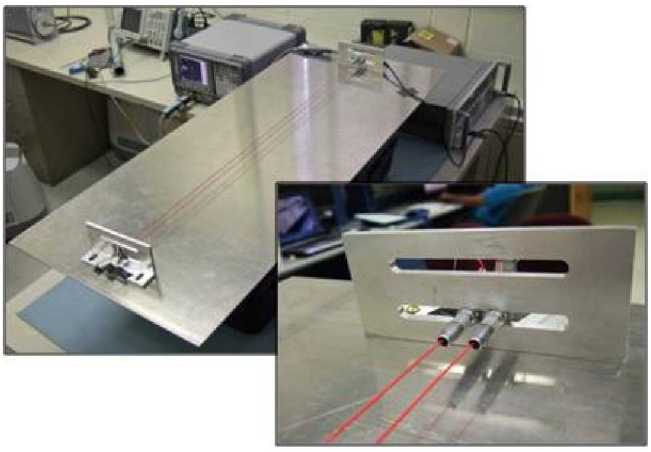

Fig. 2 Single-wire configuration test setup

wires over a large conductive sheet. An HP8657B signal generator was used to generate the stimulus V_S. Measurements were taken using an Agilent E4401B spectrum analyzer and LeCroy AP034 active differential probe.

A. Hand Calculations

As with each configuration, the system was first modeled using per-unit-length capacitances and inductances (both self and mutual). This served as a distributed lumped model representation of the electromagnetic coupling and offered a straightforward method by which to perform hand calculations and PSPICE simulations.

The expression for the voltages at each end of the receiving circuit are given by (1) and (2), where L_m and C_m are the mutual inductance and capacitance between wires. The first terms in each equation represent the inductive coupling (through loop antenna magnetic field action), and the second terms represent the capacitive coupling (through wire antenna electric field action) as discussed in [1].

$$V_{NE} = \frac{R_{NE}}{R_{NE}+R_{FE}} j\omega L_m \frac{1}{R_S+R_L} V_S + \frac{R_{NE}R_{RE}}{R_{NE}+R_{FE}} j\omega C_m \frac{R_L}{R_S+R_L} V_S \quad (1)$$

$$V_{FE} = -\frac{R_{FE}}{R_{NE}+R_{FE}} j\omega L_m \frac{1}{R_S+R_L} V_S + \frac{R_{NE}R_{RE}}{R_{NE}+R_{FE}} j\omega C_m \frac{R_L}{R_S+R_L} V_S \quad (2)$$

Total values for C_m and L_m were found by first determining the per-unit-length circuit parameters and then multiplying them by the wire length. The per-unit-length inductances and capacitances for the single wire case are given by (3)-(8) as outlined in [1].

$$l_G = \frac{\mu_o}{2\pi} \cdot \ln\left(\frac{2h_G}{r_{wG}}\right) \quad (3)$$

$$l_R = \frac{\mu_o}{2\pi} \cdot \ln\left(\frac{2h_R}{r_{wR}}\right) \quad (4)$$

$$l_m = \frac{\mu_o}{4\pi} \cdot \ln\left(1+\frac{4h_G h_R}{s^2}\right) \quad (5)$$

$$c_m = \frac{l_m}{v^2(l_G l_R - l_m^2)} \quad (6)$$

$$c_G = \frac{l_R}{v^2(l_G l_R - l_m^2)} - c_m \quad (7)$$

$$c_R = \frac{l_G}{v^2(l_G l_R - l_m^2)} - c_m \quad (8)$$

Where $\mu_o = 4\pi\times10^{-9}$ F/m is the permeability of free space, h_i is the height of the respective wire above the ground plane, r_w is the radius of a wire, s is the separation distance of the wires, ω is the angular frequency, and v is the velocity of propagation (3×10^8 m/s in free space).

B. Simulations

Simulations were completed using both PSPICE and CST's Microstripes – a time-domain field solver that uses the transmission line matrix (TLM) method. That method "meshes" the physical model in three dimensions and treats each piece as a transmission line structure.

The per-unit-length circuit model parameters calculated for hand calculations were also fed directly into PSPICE, given as Fig. 3. The inductive coupling between generator and receptor circuits was achieved using the PSPICE K-Coupling element. Capacitive coupling was achieved through the inclusion of C_M.

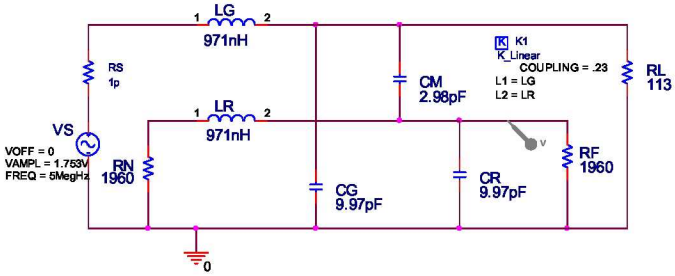

Fig. 3 PSPICE single-wire model

Microstripes was used to generate a 3D representation of the crosstalk assembly as shown in Fig. 4. The software allows the importing of CAD files or the direct drawing of physical systems. Geometries as well as the electromagnetic properties of all materials were considered during simulation.

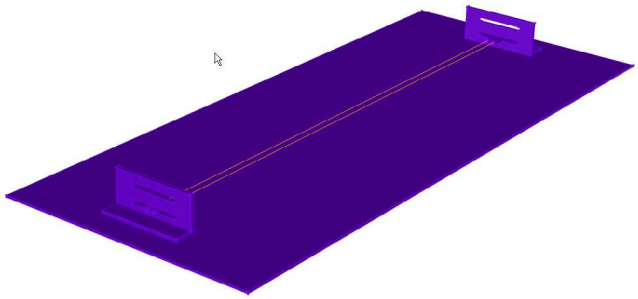

Fig. 4 Microstripes model

C. Results

For the single wire case, the results obtained from all four methods (experimentation, hand calculations, PSPICE, and

Microstripes) were all in excellent agreement. Fig. 6 and Fig. 7 show the magnitude of V_{NE} and V_{FE} for the case when R_L was varied, and R_{NE} and R_{FE} were held constant at 511Ω.

As can be seen from both graphs, there are three regions of crosstalk coupling. In the first region, R_L is small, and the inductive coupling acts as the primary crosstalk mechanism. The inverse relation between generator current and load resistance causes both the near- and far-end crosstalk voltages to decrease with increasing R_L. As R_L further increases in value, a point is reached where V_{FE} essentially goes to zero as inductive and capacitive coupling cancel. The near-end voltage on the other hand is simply the sum of the capacitive and inductive terms. Finally, in the final region, R_L becomes large enough that the capacitive term becomes the dominant coupling mechanism. This causes V_{NE} and V_{FE} to approach a constant value as can easily be seen from (1) and (2).

Fig. 8 and Fig. 9 show the results obtained when R_{NE} and R_{FE} were varied for a constant R_L, again arbitrarily chosen to be 511Ω. For simplicity, R_{NE} and R_{FE} were kept equal as they were increased. The four methods once again generally agreed quite well. Inductive coupling is the dominant mechanism for low values of R_{NE} and R_{FE}. For higher values of impedance, capacitive coupling dominates. When increasing R_{NE} and R_{FE}, the near-end crosstalk voltages increase as expected from (1). Far-end crosstalk initially decreases (negative slope) due to the cancelation between inductive and capacitive terms. Beyond that point, the slope turns positive as capacitive coupling dominates.

The trends are more intuitive when considering the simple circuit model of Fig. 1. Capacitive coupling, modeled as a constant current source, acts to inject a current into an increasing receptor impedance. This results in an increasing coupled voltage (at both ends). Likewise, for our case of a constant R_L and equal R_{NE} and R_{FE} resistors, inductive coupling remains constant and is modeled as a constant series voltage source.

III. Twisted Pair Configuration

For the second test case, the receptor wire was twisted with a return wire and grounded only at the near end. A single generator wire was routed parallel to the twisted pair. This setup was designed to emulate a real-world system in which a signal is sent to an external isolated load using twisted pair wiring.

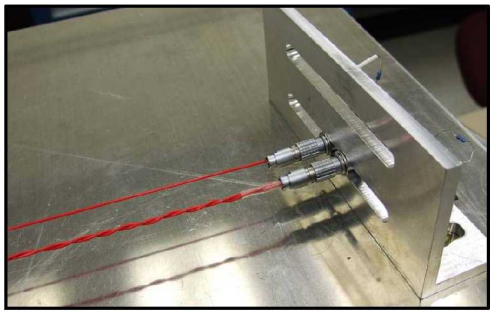

Fig. 5 Twisted Pair setup

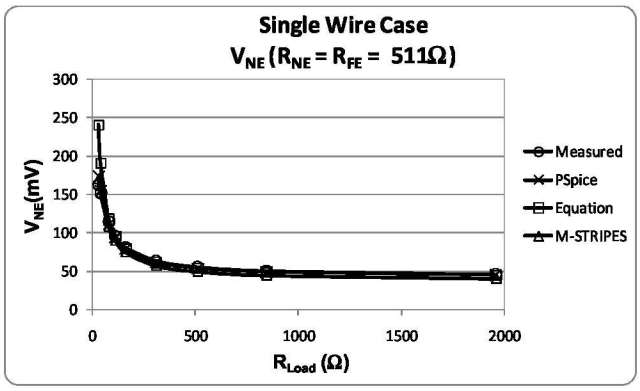

Fig. 6 V_{NE}, vary R_L, Single Wire

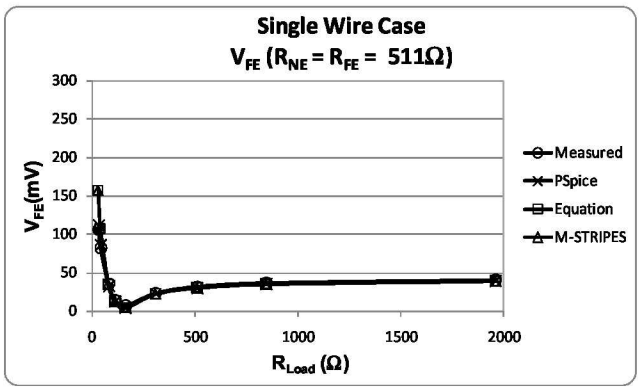

Fig. 7 V_{FE}, vary R_L, Single Wire

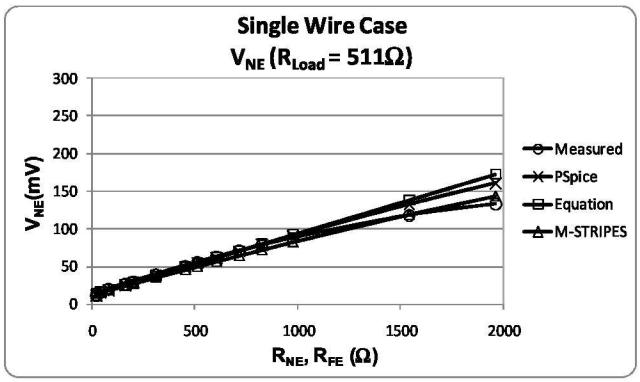

Fig. 8 V_{NE}, vary R_{NE} R_{FE}, Single Wire

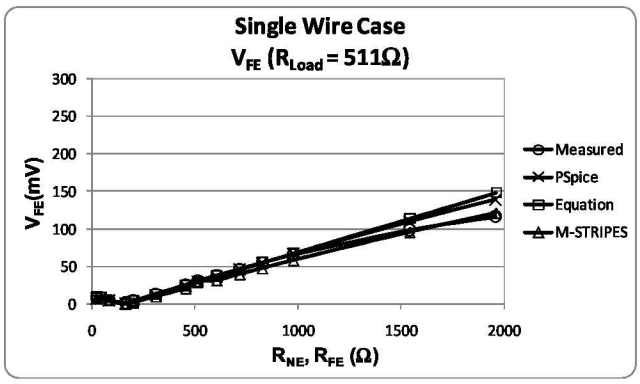

Fig. 9 V_{FE}, vary R_{NE} R_{FE}, Single Wire

The per-unit-length inductances and capacitances were once again calculated with equations presented in [1]. The near- and far-end voltages are then given by (9) and (10).

$$V_{NE} = \left[\frac{R_{NE}}{R_{NE}+R_{FE}} j\omega(l_{m1}-l_{m2})\mathcal{L}_{HT}\frac{1}{R_S+R_L}V_S\right] + \left[\frac{R_{NE}R_{FE}}{R_{NE}+R_{FE}} j\omega c_m \mathcal{L}\frac{R_L}{R_S+R_L}V_S\right] \quad (9)$$

$$V_{FE} = \left[\frac{-R_{FE}}{R_{NE}+R_{FE}} j\omega(l_{m1}-l_{m2})\mathcal{L}_{HT}\frac{1}{R_S+R_L}V_S\right] + \left[\frac{R_{NE}R_{FE}}{R_{NE}+R_{FE}} j\omega c_m \mathcal{L}\frac{R_L}{R_S+R_L}V_S\right] \quad (10)$$

The PSPICE model is given as Fig. 10.

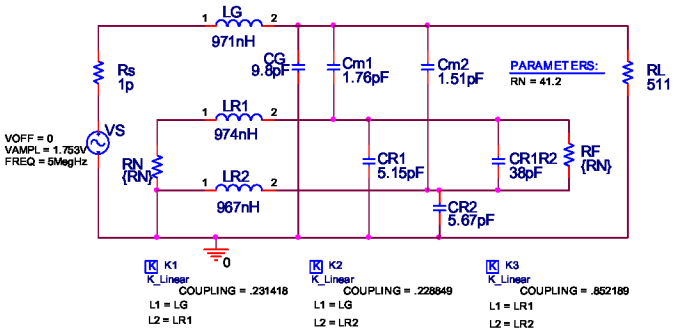

Fig. 10 PSPICE model of twisted pair

From basic field theory, one would expect a reduction in crosstalk due to the use of a dedicated return wire. With a smaller primary current loop area, the total magnetic flux coupled into the receptor circuit is greatly reduced. Furthermore, there is an additional decrease in magnetic field coupling due to the alternating polarity of each loop. Induced voltages in one loop would be expected to cancel out the induced voltages in the adjacent loop.

The results of the twisted pair case were again consistent between calculations, simulations, and experimentation. Also as expected, the data revealed that the use of a twisted dedicated return greatly reduced inductive coupling. Fig. 11 and Fig. 12 show that for a fixed R_{NE} and R_{FE}, all that remains is the modest level of capacitive coupling. Likewise, Fig. 13 and Fig. 14 show the expected positive trend without the earlier dip seen as a result of inductive-capacitive cancellation.

IV. Summary

In this first part, crosstalk into a single wire above a ground plane and into twisted pair wiring was examined. For both cases, hand calculations, PSPICE, Microstripes, and empirical data agreed very well. Additional cases are examined in Part 2.

V. References

[1] C.R. Paul, *Introduction to Electromagnetic Compatibility*, 2nd ed., Wiley Interscience, New Jersey, 2006.

[2] H.W. Ott, *Noise Reduction Techniques in Electronic Systems*, 2nd ed., Wiley Interscience, New York, 1988.

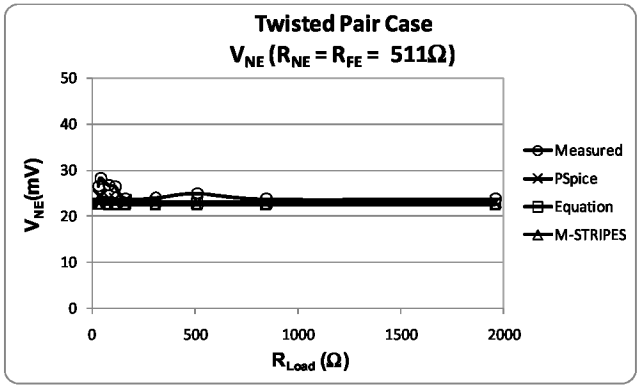

Fig. 11 V_{NE}, vary R_L, Twisted Pair

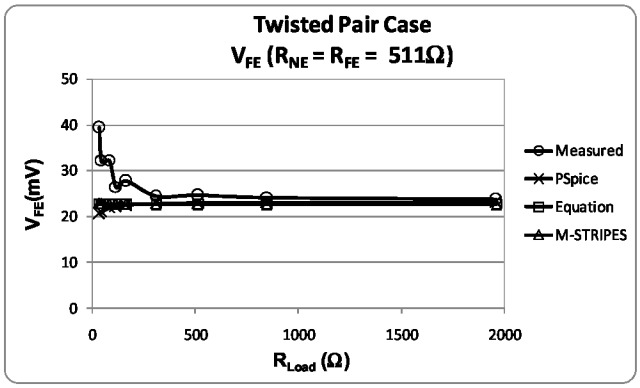

Fig. 12 V_{FE}, vary R_L, Twisted Pair

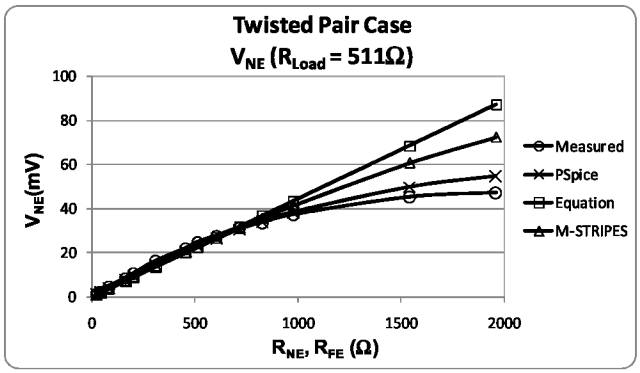

Fig. 13 V_{NE}, vary R_{NE} R_{FE}, Twisted Pair

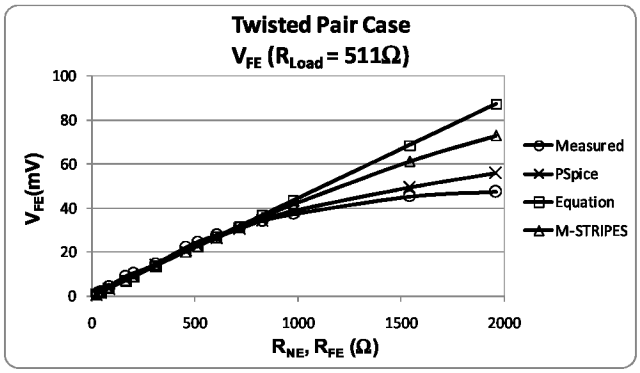

Fig. 14 V_{FE}, vary R_{NE} R_{FE}, Twisted Pair